




Article

Modeling Desorption Rates and Background Concentrations of Heavy Metals Using a One-Dimensional Approach

Wendy Tatiana Gonzalez Cano ^{1,2,3} , Serguei Lonin ³  and Kyoungrean Kim ^{1,2,*} 

¹ Marine Environmental Research Department, Korea Institute of Ocean Science and Technology, Busan 49111, Republic of Korea; tatiana@kiost.ac.kr

² KIOST School, University of Science and Technology (UST), Busan 49111, Republic of Korea

³ Admiral Padilla Naval Academy of Cadets, Isla Naval Manzanillo, Cartagena de Indias 130001, Colombia; oceanmet.ltda@yahoo.com

* Correspondence: kyoungrean@kiost.ac.kr; Tel.: +82-51-664-3198

Abstract: Harmful heavy metals (HHMs) in marine sediments pose significant ecological and human health risks. This research developed a novel one-dimensional mathematical model to investigate the desorption rates and background concentrations (C_{bg}) of HHMs in cohesive sediments of coastal environments, using Cartagena Bay (CB), Colombia, as a reference for estuarine systems. The model integrates mass balance and molecular diffusion equations incorporating porosity and tortuosity. Both the particulate and dissolved phases of HHMs were considered. Numerical experiments were conducted over 28 years with a daily time step, simulating four primary hydrodynamic processes: molecular diffusion, desorption, sedimentation, and turbulent water exchange. The spatiotemporal evolution of C_{bg} provides valuable insights for sediment modeling, policy development, and advancing the understanding of HHM pollution in sediments. Results of the model align closely with empirical data from CB, demonstrating its applicability not only to local conditions but also to similar contaminated areas through a generalized approach. This model can be used as a reliable computational tool for managing coastal environments.

Keywords: estuarine sediments; heavy metals; background concentrations; desorption rate; cohesive sediment transport; mathematical modeling



Academic Editor: Daochen Zhu

Received: 28 April 2025

Revised: 16 May 2025

Accepted: 19 May 2025

Published: 22 May 2025

Citation: Gonzalez Cano, W.T.; Lonin, S.; Kim, K. Modeling Desorption Rates and Background Concentrations of Heavy Metals Using a One-Dimensional Approach. *Toxics* **2025**, *13*, 421. <https://doi.org/10.3390/toxics13060421>

Copyright: © 2025 by the authors. Licensee MDPI, Basel, Switzerland. This article is an open access article distributed under the terms and conditions of the Creative Commons Attribution (CC BY) license (<https://creativecommons.org/licenses/by/4.0/>).

1. Introduction

Heavy metal pollution poses a global environmental concern due to its severe toxicity [1,2], long-term persistence, and bioaccumulation in food chains [3–5]. Harmful heavy metals (HHMs) are continuously introduced into the environment [6] through natural and anthropogenic sources [7,8]. In estuarine waters, the presence of HHMs is generally observed in two distinct phases: dissolved in the water column and particulate adsorbed on the sediments. The partitioning of HHMs between these phases depends on the physical and chemical characteristics of suspended particles [9,10], in conjunction with environmental conditions such as salinity, pH, and dissolved organic matter [10].

Upon entering surface waters, HHMs are transported by rivers through wash load transport and eventually accumulate in marine sediments. Hydro-sedimentary processes such as desorption [11], resuspension, and dredging can release these contaminants back into the overlying water column [12], affecting water quality, the marine environment, and human health. Although HHM adsorption initially occurs near areas with significant anthropogenic activities, this study emphasizes the downstream consequences, particularly focusing on sediment contamination.

Various researchers rely on predicting interactions between water and sediments as a critical method for understanding HHM pollution [5,13–15]. Mathematical models have become powerful tools to address complex research questions related to coastal environments, offering reliable, cost-effective, and time-saving approaches [16].

Specifically, reaction-transport models, as described by Boudreau [17], Lynch and Officer [18], and Nicolis [19], have been pivotal in advancing sediment diagenesis and biogeochemical modeling, integrating key processes such as molecular diffusion, advection, and chemical reactions. These frameworks form the theoretical foundation of this study, focused on the vertical distribution and temporal evolution of HHMs in sediments.

Previous studies, such as Wu et al. [10], developed a two-dimensional (2D) transport model, later integrated into a one-dimensional (1D) framework to simulate the movement of dissolved and particulate HHMs along estuaries. However, these models did not explicitly address the accumulation of HHM contaminants or their subsequent phase evolution within the substrate, a significant gap in understanding the long-term impacts and interactions of HHMs with sediment dynamics.

Numerous studies have focused on HHM accumulation in sediments near contamination sources. However, limited studies have been published on desorption rates and their dynamics in downstream depositional environments such as lakes, lagoons, and estuaries. In systems dominated by wash load transport of fine cohesive sediments, the deposition and accumulation pathways of metal-bearing particles are not well documented. Apparently, sediment accumulation may occur slowly in distal areas, comparable to sorption rates, or rapidly near river mouths due to abrupt precipitation of materials, limiting metal exchange with the water column. These spatial heterogeneities affect HHM redistribution within sediments, complicating the estimation of background concentrations (C_{bg}).

This study advances existing frameworks by proposing a novel 1D model that couples transport and reaction processes. This model is designed for application at each computational node of a generalized three-dimensional (3D) hydrodynamic model, serving as a boundary condition at the water–sediment interface to simulate HHM accumulation and sediment evolution over time. The innovation of this approach is the integration of both dissolved and particulate HHM phases. Four critical hydrodynamic processes are quantified and modeled to evaluate their influence on HHM dynamics. This model, in accordance with empirical data, assumes that the dissolved-phase concentration (C_d) is considerably lower than the particulate-phase concentration (C_p) in the water column ($C_d \ll C_p$).

To demonstrate the model's applicability, simulations were referenced against estuarine conditions in the Cartagena Bay, Colombia (CB), a system subject to intense sedimentation and HHM inputs. Results obtained through this model align closely with empirical observations, reinforcing its validity.

The aim of this study is (1) to develop a novel 1D mathematical model to investigate HHM dynamics in estuarine sediments and (2) to elucidate the processes of HHMs governing background concentrations (C_{bg}). These concentrations serve as critical indicators for identifying anthropogenic inputs [20] and facilitate the formulation of effective management and remediation strategies [7,21]. This research represents the first attempt to establish the C_{bg} of HHMs in Colombia, highlighting its significance in addressing local and regional environmental concerns.

The model is applicable beyond the specific conditions of the Colombian coastline and could be effectively extended to various aquatic systems, including rivers, estuaries, and lakes worldwide affected by sediment contamination. Model outputs, including dynamic profiles illustrating the temporal drift of C_{bg} , are presented and critically discussed.

2. Materials and Methods

2.1. Cartagena Bay: A Reference System for Estuarine Conditions

CB is a semi-enclosed estuarine system on Colombia's Caribbean coast (Figure 1) ($10^{\circ}16'–10^{\circ}26' \text{ N}$, $75^{\circ}30'–75^{\circ}35' \text{ W}$), with an average depth of 16 m, a maximum depth of 32 m, and a surface area of 84 km^2 [22]. The bay receives large amounts of sediments [23], nutrients, wastewater runoff [24], and contaminants from the Dique Channel [25,26], an artificial structure connected to the extensive Magdalena River basin ($260,000\text{-km}^2$) [26,27].

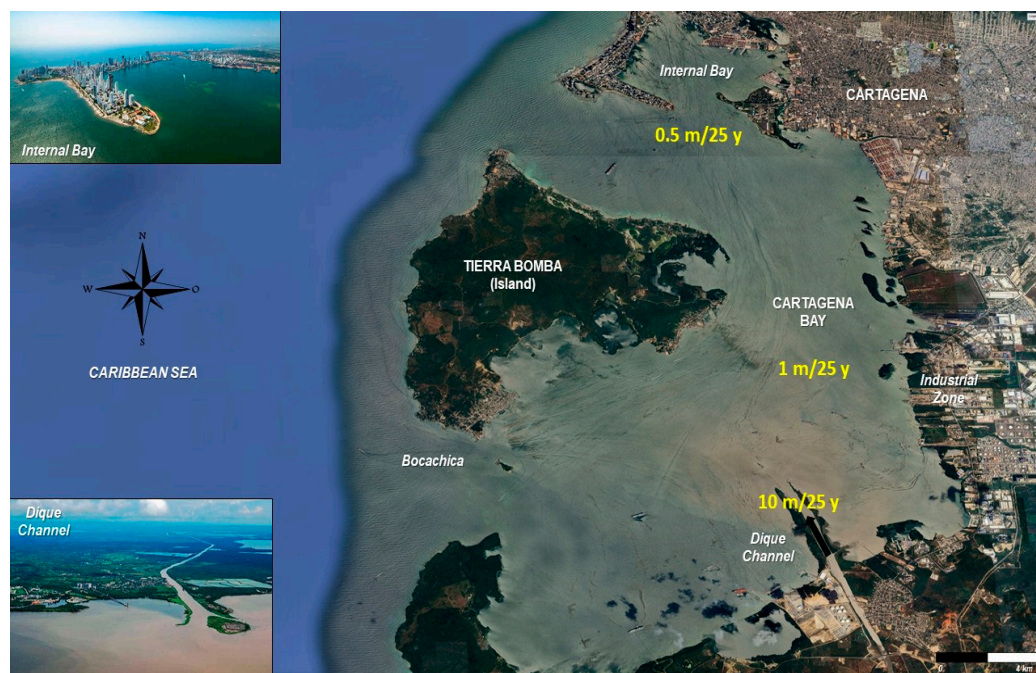


Figure 1. Location of the Cartagena Bay, Colombia ($10^{\circ}24' \text{ N}$, $75^{\circ}30' \text{ W}$), showing the variability of sedimentation across the bay with three estimated deposition rates: Dique Channel mouth: $10 \text{ m}/25 \text{ y}$; the central bay: $1 \text{ m}/25 \text{ y}$; and the northern sector: $0.5 \text{ m}/25 \text{ y}$. The Dique Channel is highlighted as the main sediment input pathway. Source: authors, modified from Google Earth; pictures taken from Google Images (accessed May 2025).

The Magdalena River transports a sediment flux of 184 Mt yr^{-1} and delivers the highest freshwater discharge ($6496 \text{ m}^3 \text{ s}^{-1}$) and sediment load (144 Mt yr^{-1}) to the Caribbean [26,27]. Seasonal rainfall from the Magdalena River, where the Dique Channel diverges, strongly influences the hydrology and sediment quality of CB [28]. CB's sedimentation patterns and morpho-dynamic characteristics have been previously studied through observations and modeling [29–31]. Due to wash load transport, HHM adsorption does not occur in CB but rather in distant sources before HHMs are transported downstream. This explains the HHM accumulation in precipitated sediments.

2.2. Mathematical Model

2.2.1. Definition of the Physical Problem

This research considers the wash load transport [32] of fine cohesive sediments (silt and clay) loaded with HHMs in particulate form. The primary source of HHMs is the rapid upstream industrialization in the Magdalena River. Particles are deposited at the bottom in the form of flocs. In the porous medium of precipitated sediments, desorption continues but at a lower rate than that during transport in the water column.

In the water column, HHMs exist in colloidal, particulate, and dissolved phases. The concentration of HHMs in dissolved form (C_d) is generally lower than that in particulate

form (C_p). For instance, field measurements in the Magdalena River show that C_d values are approximately 1000 times lower than C_p in suspended and bottom sediments. This aligns with observations by Bartlett and Craig (1981) [33], who reported strong correlations ($r = 0.94$) between mercury (Hg) and silt in British estuaries, demonstrating Hg's affinity for fine particles and sulfur-rich organic matter (<0.0625 mm). The volumetric concentration of suspended sediments at the transition between dilute and concentrated systems is typically below 10^{-4} (dimensionless). Considering that desorption occurs over several years (~ 6 years), the mass of HHMs released from particulates is dispersed into a much larger water volume, further supporting the assumption $C_d \ll C_p$. Combined with the infinite-dilution diffusion concept [34], these theoretical and empirical insights justify the assumption as a valid simplification within this modeling framework.

Hereafter, we assume that C_d concentrations are multiplied by the constant K_d , which represents the equilibrium distribution coefficient. In the sediment substrate, these concentrations are also assumed to reach equilibrium due to limitations in molecular diffusion, which is partially restricted by porosity (n) and tortuosity (θ). Lower porosity and higher tortuosity restrict molecular diffusion, reducing HHM exchange with overlying waters and consequently promoting high accumulation and persistence within the sediment layer.

Tortuosity quantifies the complexity of pore pathways through which water and dissolved substances, such as HHMs, move within sediment layers [35]. Porosity, defined as the ratio of pore volume to total sediment volume [17], also plays a critical role in transport dynamics. Lower porosity implies fewer and smaller pores, restricting mobility and facilitating contaminant accumulation. As sediment compacts over time, porosity typically decreases with depth (z), becoming a time-dependent function. This leads to a gradual increase in substrate thickness in the absence of resuspension.

The desorption rate (γ), reflects the release of HHMs from C_p to C_d and depends on the grain diameter of sediments (d_{50}), their porosity (n), salinity (S), and pH. The porosity and tortuosity together influence molecular diffusion, calculated in the model using the Schmidt number (Sc), a dimensionless parameter used to characterize the relationship between the molecular viscosity of water and the diffusion of substances [36].

A 1D vertical model was formulated, neglecting the horizontal dispersion of HHMs, with the vertical axis directed upward from $z = 0$ (the reference level is assumed to be the starting point of sedimentation, as shown in Figure 2). The 1D model can be considered a sufficient approximation, considering that (a) the relationship between the vertical scale of the sediment layer and its horizontal extent along an estuary or river is small, and (b) exchange processes in the substrate in the vertical direction are much faster than the horizontal dynamics.

The domain is defined as $\{0 \leq z \leq D(t); t \geq 0\}$, where D = sediment thickness as a function of time (t). At the initial time, D was set as $D(t = 0) = 0$. To avoid singularities when solving the differential equations of the model, we assumed that $\frac{\partial D}{\partial t} > 0, \forall t$ under the absence of resuspension. The dynamics of the layer $D(t)$ are expressed as follows:

$$\frac{\partial D}{\partial t} = -w_g C_v (1 - n)^{-1} = \frac{-w_g (1 - n)^{-1} C_m}{\rho_s}, \quad (1)$$

where w_g is the settling velocity of sediments due to gravity, given by the Stokes formula ($w_g < 0$), and C_v , C_m , and ρ_s are the volumetric and mass concentrations of suspended sediments and their density, respectively. Within the bottom substrate, the molecular diffusion flux of the C_d is defined as follows:

$$Q = \alpha_s v \frac{\partial C_d}{\partial z}, \quad (2)$$

where ν is the kinematic molecular viscosity of water (Constant) and α_S defines the inverse Schmidt number ($\alpha_S = Sc^{-1}$) [36], which generally depends on time and substrate level or porosity n .

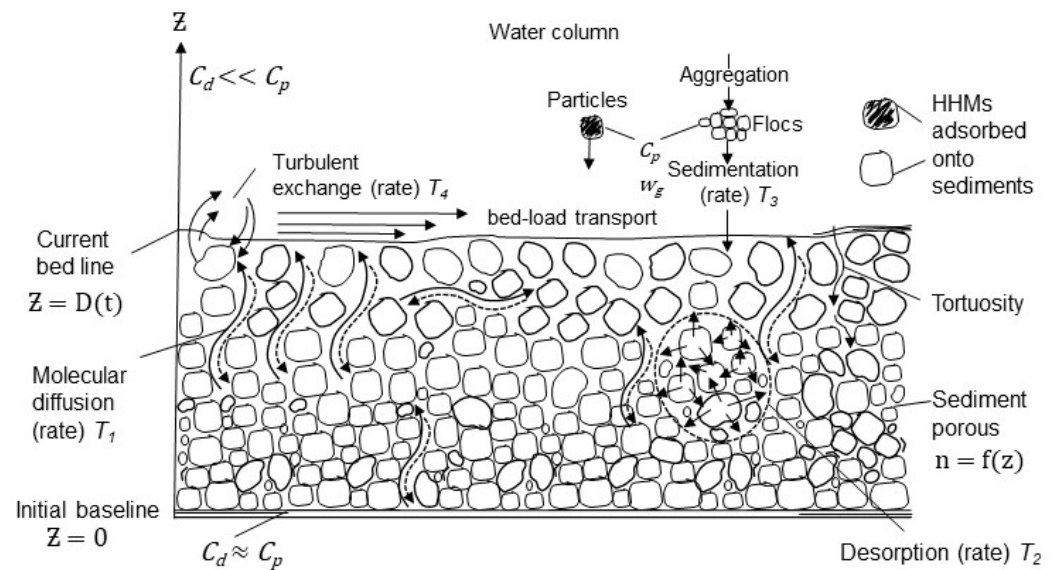


Figure 2. Conceptual model of HHM dynamics at the water–sediment interface and within the sediment substrate.

To determine the desorption rate $\gamma = f(d_{50}, n, S, pH)$, at least three timescales must be considered: (1) the molecular diffusion rate (T_1) of HHMs; (2) the desorption rate (T_2); and (3) the sediment deposition rate (T_3) at the bottom, as follows:

$$T_1 = \frac{D_0^2 Sc}{\nu}, \quad (3)$$

$$T_2 = \frac{1}{2\gamma}, \quad (4)$$

$$T_3 = \frac{D_0}{w_g C_v}. \quad (5)$$

This study has focused on the formulation and evaluation of a generalized 1D model for simulating HHM behavior in estuarine sediments, rather than on site-specific applications. The parameters of the model, particularly sedimentation and desorption rates, were calibrated within observed HHM concentrations reported in empirical data from CB [24,25,27,37]. The mathematical model was implemented and numerically solved using FORTRAN 90. Model outputs were compared to published sediment data from CB [23–25,38]. Simulated C_{bg} ranging from 1.0–2.4 mg kg^{−1} dw closely matched these empirical values at the sediment base ($z = 0$). The median grain diameter (d_{50}) (Table 1) was measured using a laser diffraction particle size analyzer. HHM concentrations were determined in the collected data using standard laboratory procedures involving acid digestion followed by quantification via atomic absorption spectrometry (AAS) or inductively coupled plasma mass spectrometry (ICP-MS). Although full calibration was limited by data availability, alignment with observed depth-integrated values provides partial validation.

Table 1. State variables and parameters used in this study.

Parameter	Description	Unit	Value	Reference
C_{bg}	HHM background concentration	g L^{-1} , mg kg^{-1} (dw) *	see Table 2	calculated
C_D	Drag coefficient	/	2×10^{-3}	[39]
C_d	Dissolved-phase HHM concentration	g L^{-1} , mg kg^{-1} (dw) *	/	calculated
C_m	Suspended-sediment mass concentration	g L^{-1}	/	[40]
C_p	Particulate-phase HHM concentration	g L^{-1} , mg kg^{-1} (dw) *	/	calculated
C_{p0}	Initial particulate HHM at precipitation	g L^{-1}	/	assumed
C_v	Suspended-sediment volumetric concentration	/	10^{-4} – 10^{-5}	assumed
d_{50}	Median grain diameter of sediment	m	/	measured
D	Sediment thickness	m	0–1.6 **	calculated
F	Porosity–tortuosity factor	/	/	calculated
HHMs	Harmful heavy metals	g L^{-1} , mg kg^{-1} (dw) *	varies	measured
K_d	Coefficient of equilibrium distribution	/	/	assumed
m	Exponent in the relationship of Sc and n	/	/	literature
N	Number of computational nodes	/	100	assumed
n	Porosity	/	0.4	[34]
Q	Molecular diffusion flux	$\text{kg m}^{-2} \text{s}^{-1}$	varies	calculated
S	Salinity	/	0.06–35.7	assumed
Sc	Schmidt number	/	10–100	[6]
t	Time	s	0 – 8.64×10^8 s	assumed
T_1	Molecular diffusion rate	yr	0.3–3	calculated
T_2	Desorption rate	yr	3.15 (for $\gamma = 5 \times 10^{-8}$)	calculated
T_3	Sediment rate	yr	>31	calculated
T_4	Turbulent exchange rate	yr	/	calculated
u_*	Friction (dynamic) velocity	m s^{-1}	0–0.01	assumed
w_g	Settling velocity of sediments due to gravity	m s^{-1}	10^{-5}	assumed
Y	Dimensionless vertical coordinate	/	0–1	calculated
z	Vertical level within the substrate	m	0–1.6	calculated
z_0	Roughness parameter	m	/	literature
α_S	Inverse Schmidt number (Sc^{-1})	/	0.01–0.1	[36]
γ	Desorption coefficient	s^{-1}	5×10^{-8} – 1×10^{-9}	[41]
Δy	Vertical grid size in dimensionless coordinates	/	$1/(N - 1)$	calculated
θ	Tortuosity	/	/	[35]
κ	Karman constant	/	0.41	literature
ν	Kinematic molecular viscosity of water	$\text{m}^2 \text{s}^{-1}$	10^{-6}	constant
ρ_s	Sediment–particle density	kg m^{-3}	2650	[39]
χ_0	Molecular diffusion coefficient (water only)	$\text{m}^2 \text{s}^{-1}$	/	[17]
χ_s	Molecular diffusion coefficients (with sediments)	$\text{m}^2 \text{s}^{-1}$	/	calculated

* C_d and C_p represent concentrations expressed in g L^{-1} or kg m^{-3} in the model for consistency, but in the figures, they are presented in mg kg^{-1} dry weight (dw) for easier comparison with laboratory data. Laboratories generally measure HHM concentrations in mg kg^{-1} , dw. Note that this difference in units is important when interpreting model results and comparing them with laboratory data or figures. ** D (0–1.6 m) based on 28 years of sedimentation. “/” means no value.

Four numerical simulation scenarios (Cases 1–4) were analyzed to investigate the influence of hydrodynamic parameters on HHM accumulation dynamics. Case 1 ($\gamma = 5 \times 10^{-8} \text{ s}^{-1}$) represents relatively fast desorption conditions, whereas Case 2 ($\gamma = 10^{-8} \text{ s}^{-1}$) examines the system response under slower desorption dynamics. Case 3 simulates a time-dependent increase in the C_p of HHMs, linearly increasing from 0 to 2.4 mg kg^{-1} over 28 years, reflecting observed historical contamination trends from distant sources such as the Magdalena River. Case 4 incorporates variable sediment inputs (55 – $250 \text{ m}^3 \text{ s}^{-1}$), modeled through stochastic annual fluctuations to replicate seasonal variations typical of the Dique Channel. These scenarios evaluate sedimentation and desorption processes under contrasting environmental conditions with broader applicability.

Table 2. Model-derived Hg background concentrations (C_{bg}) at boundary ($z = 0$) under different simulation cases.

Case	Description	Estimated C_{bg} mg kg^{-1} (dw)	Observation
1	$\gamma = 5 \times 10^{-8} \text{ 1/s}$	1.4–1.7	Long-term equilibrium at $z = 0$
2	$\gamma = 10^{-8} \text{ 1/s}$	1.0–1.2	Slower equilibrium from low γ
3	C_{p0} increasing over 28 yr	2.0–2.4	Closest to observed CB field data
4	Variable sediment input *	2.0–2.2	Dynamic but consistent C_{bg} at $z = 0$
-	Average Hg C_{bg} (model)	0.2 ± 1.7	Variability across all cases

* Seasonal sediment variation using white noise flow $55\text{--}250 \text{ m}^3 \text{ s}^{-1}$.

2.2.2. Governing Equations and Boundary Conditions

The mathematical formulation of the problem is expressed in Equation (1). The governing equations for C_p and C_d of HHMs are defined clearly below (Equations (6) and (7)), including mass balance constraints and desorption processes:

$$\frac{\partial C_p}{\partial t} = -\gamma(C_p - C_d) - \frac{w_g}{D} C_{p0} \delta(z - D) \quad (6)$$

$$\frac{\partial C_d}{\partial t} = \gamma(C_p - C_d) + \frac{\partial}{\partial z} \left(\alpha_s v \frac{\partial C_d}{\partial z} \right), \quad (7)$$

$$AC_d + \alpha_s v \frac{\partial C_d}{\partial z} = 0, \text{ at } z = D(t) \quad (8)$$

$$\frac{\partial C_d}{\partial z} = 0, \text{ at } z = 0 \quad (9)$$

In Equation (8), A is a constant defined in Appendix B, based on the fact that in the water column, $C_d \ll C_p$ due to diffusion in open water systems. As stated by the no-flux condition in Equation (9), an asymptotic equilibrium is assumed at $z = 0$ between C_p and C_d , with values equal to the C_{bg} to be defined in this study.

This boundary condition assumes equilibrium at lower sediment layers ($z = 0$), reaching a balance due to decreased porosity and restricted molecular diffusion over time. In Equation (9), the molecular flux of C_d at $z = 0$ is assumed to be zero. The boundary conditions at $z = 0$ and $z = D(t)$ ensure the mass balance of HHMs within the sediment, accurately representing fluxes and the conservation of mass. At $z = D(t)$, the boundary condition models the exchange between the sediment and the overlying water column.

2.2.3. Numerical Solution Under Variable Boundary Conditions

Equations (6)–(9), with their respective initial conditions of $C_p(z, t = 0) = C_d(z, t = 0) = 0$, have a variable boundary at an initial thickness of $D(t = 0) = 0$. The vertical coordinate (z) was transformed into a non-dimensional coordinate, following Yao et al. [13], to improve numerical solution robustness. The system herein was reformulated using a new variable:

$$y = \frac{z}{D(t)}$$

This becomes $y_j = (j - 1)\Delta y$; $j = 1, \dots, N$; $\Delta y = \frac{1}{N-1}$, where N is the number of vertical computational nodes. Thus, combining Equations (6) and (7) with Equation (1), we obtain the following:

$$\frac{\partial C_p}{\partial t} + \frac{y}{D} \frac{w_g C_V}{(1 - n)} \frac{\partial C_p}{\partial y} = -\gamma(C_p - C_d) - \frac{w_g}{D} C_{p0} \delta(z - D), \quad (10)$$

$$\frac{\partial C_d}{\partial t} + \frac{y}{D} \frac{w_g C_V}{(1-n)} \frac{\partial C_d}{\partial y} = \gamma(C_p - C_d) + \frac{\nu}{D^2} \frac{\partial}{\partial y} \left(\alpha_s \frac{\partial C_d}{\partial y} \right). \quad (11)$$

These equations were then discretized using an implicit time scheme, ensuring numerical stability regardless of the sediment thickness, D . The first derivatives concerning y were then represented using an “upward” scheme of $O(\Delta y^1)$. The solution was obtained using the Thomas factorization algorithm.

3. Results

3.1. Estimation of Molecular Diffusion (T_1), Desorption (T_2), and Sedimentation (T_3)

To estimate the timescales (T_1 , T_2 , T_3) given by Equations (3)–(5), a characteristic sediment thickness ($D_0 = 1$ m), molecular viscosity ($\nu = 10^{-6} \text{ m}^2 \text{ s}^{-1}$), and Schmidt number ($Sc = 100$) were adopted [6]. With these parameters, T_1 was estimated to be 3 years. For $Sc = 10$, T_1 was approximately 115 days. According to Liu et al. [42], the values of γ vary between 10^{-8} and 10^{-9} s^{-1} . For $\gamma = 5 \times 10^{-8} \text{ s}^{-1}$, the timescale of T_2 was 3.15 years.

Finally, assuming that the volumetric concentration was between 10^{-4} and 10^{-5} and the settling velocity due to gravity was 10^{-5} m/s , the value of T_3 was greater than 31 years. Therefore, $T_3 \gg \max(T_1, T_2)$. T_3 has the slowest timescale, while the other two timescales were similar to each other.

In addition to previously defined timescales (T_1 – T_3), a fourth timescale (T_4), representing the turbulent water column exchange of dissolved HHMs at the sediment–water interface, was determined. Resuspension was not considered, as particulate-bound HHMs do not significantly participate in this exchange.

3.2. Numerical Experiments

The sediment density (ρ_s) was set at 2650 kg m^{-3} , with porosity (n) fixed at 0.4. A drag coefficient (C_D) of 2×10^{-3} [39] and an initial dynamic velocity of 0.01 m s^{-1} were applied. Numerical experiments were conducted over 28 years, using a daily time step (1 d). Figure 3 illustrates the temporal evolution of C_d and C_p from the beginning of precipitation on both the surface and base when the desorption coefficient γ is varied. Sedimentation was assumed to continue uniformly over the 28-year simulation at constant rates, with fixed HHM concentrations in the precipitated sediments. In Figure 4, profiles of HHM concentrations in sediments are presented at both the midpoint and the end of the numerical experiments.

Over 28 years, the sediment layer grew to 1.6 m, which aligned well with data from CB and served as a reference for this study. Following an initial transient period (Figure 3), the C_d and C_p stabilized. The desorption rate was slower, corresponding to 6.3 years on the timescale of this process, compared to the reference value of 3.15 years.

The vertical profiles exhibited an exponential variation in the upper layer of the substrate (Figure 4), over 30–40 cm, followed by a uniform distribution. The variation was attributed to the vertical molecular diffusion of HHMs and their loss, particularly in C_d , due to turbulent exchange with the water column at the bottom. The uniform distribution in the lower sublayer indicates equilibrium between the two phases; however, this equilibrium was not constant (Figure 4). Equilibrium stability between C_d and C_p is crucial for ecological risk assessments, as it governs HHM bioavailability and potential toxicity in benthic ecosystems [43].

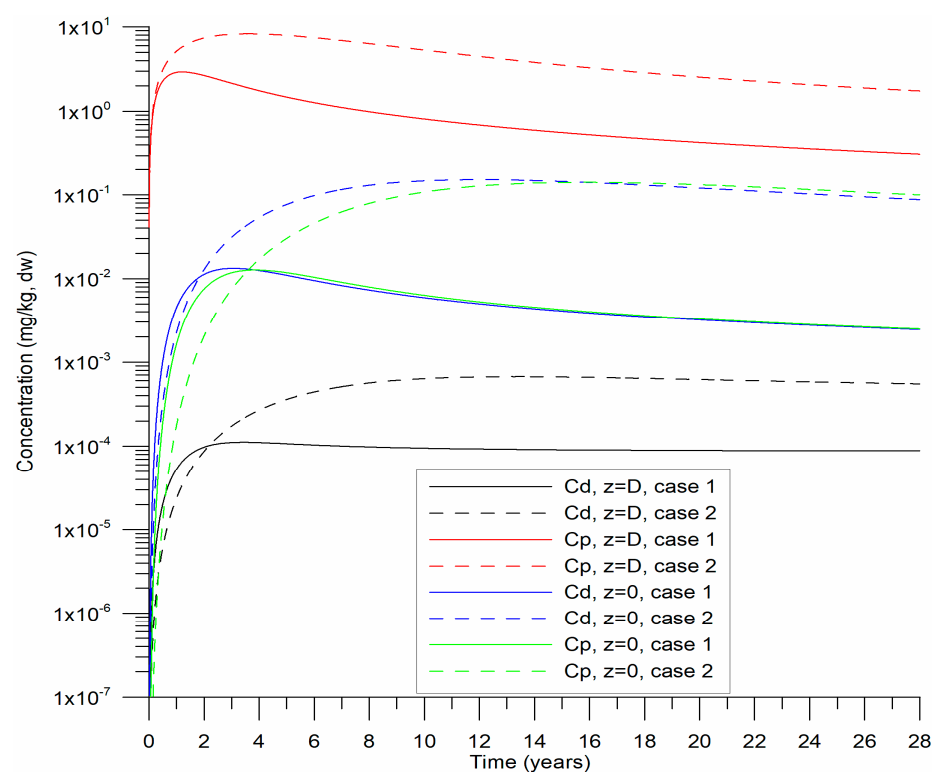


Figure 3. Temporal evolution of particulate (C_p) and dissolved (C_d) HHM concentrations at the variable bed level $D(t)$ and the basal level ($z = 0$) of the bottom substrate for Cases 1 and 2.

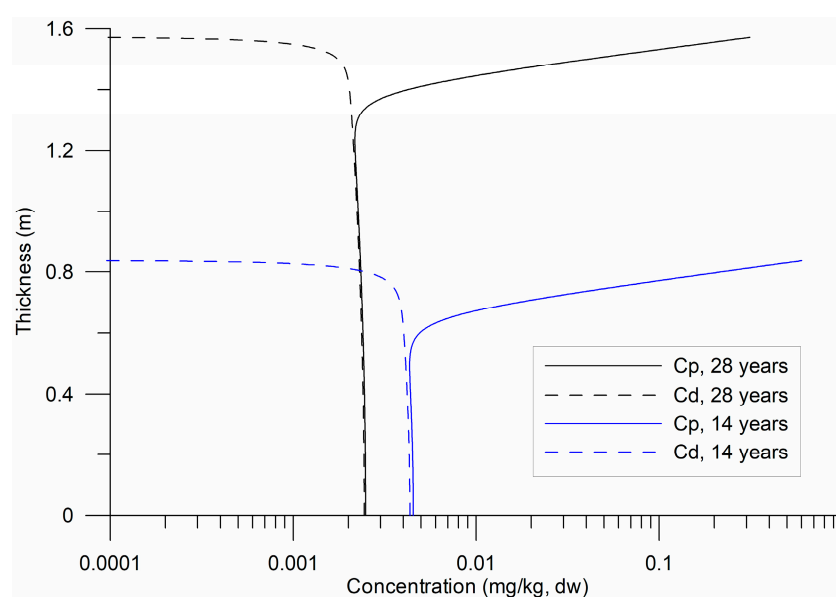


Figure 4. Temporal variability in the vertical profiles of particulate (C_p) and dissolved (C_d) HHMs for 14 and 28 years of sedimentation ($\gamma = 5 \times 10^{-8} \text{ s}^{-1}$).

4. Discussion

4.1. Temporal Evolution of Background Concentrations Estimated by the Model

A drift value, tentatively called the background C_{bg} , was observed, characterized by a gradual decrease over time. This decrease is attributable to continuous slow molecular diffusion within the non-zero sediment porosity, transporting HHMs towards the sediment–water interface. Subsequent experiments were conducted by minimizing the turbulent exchange of the C_d with the water column above the bed. This occurs when $u_* \rightarrow 0$

(Figure 5). A nearly uniform distribution of C_d in the vertical direction was observed, along with the input of C_p at the bottom surface. The total concentrations of HHMs in the sediments were the sum of C_p and C_d/K_d , and in the laboratory, a single value was defined: “HHM concentrations in sediments”.

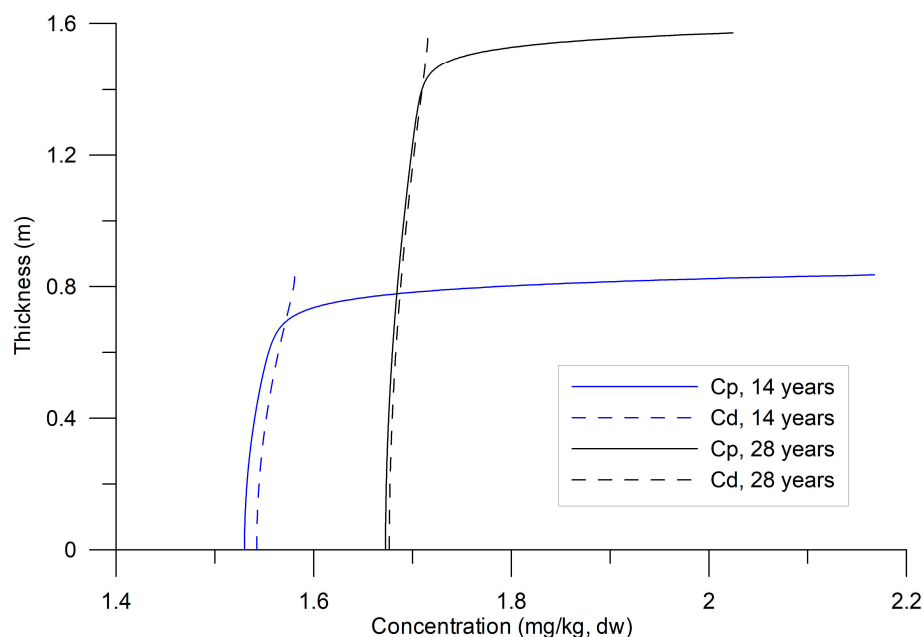


Figure 5. HHM concentrations in sediments under conditions of limited exchange between the dissolved phase and the water column.

For Case 1, γ was set to $5 \times 10^{-8} \text{ s}^{-1}$, which suggested a relatively faster desorption rate compared to Case 2 ($\gamma = 10^{-8} \text{ s}^{-1}$). Two additional cases (Cases 3 and 4) were simulated (Figure 6). In Case 3, the initial particulate concentration C_{p0} , increased linearly from 0 to 2.4 mg kg^{-1} over 28 years, reflecting observed trends in CB associated with increased HHM loading from a distant source, the Magdalena River. Case 4 was similar to Case 3, but with a variable sediment input that varied between 55 and $250 \text{ m}^3 \text{ s}^{-1}$ to replicate the Dique Channel’s seasonal flow, using annually periodic white-noise perturbations (stochastic values 0–1).

The cases in Figure 6 were compared to Case 1 in Figure 3 where HHMs in sediments accumulated more slowly. Notably, when HHM loading gradually increased (Case 3), the concentrations at the sediment base ($z = 0$) consistently reached equilibrium ($C_d = C_p = C_{bg}$). Conversely, seasonal variations in sediment load from the Dique Channel (Case 4) did not significantly alter the equilibrium C_{bg} value. These findings imply that C_{bg} values remain stable despite short-term fluctuations, highlighting their value as robust indicators for long-term ecological risk assessments.

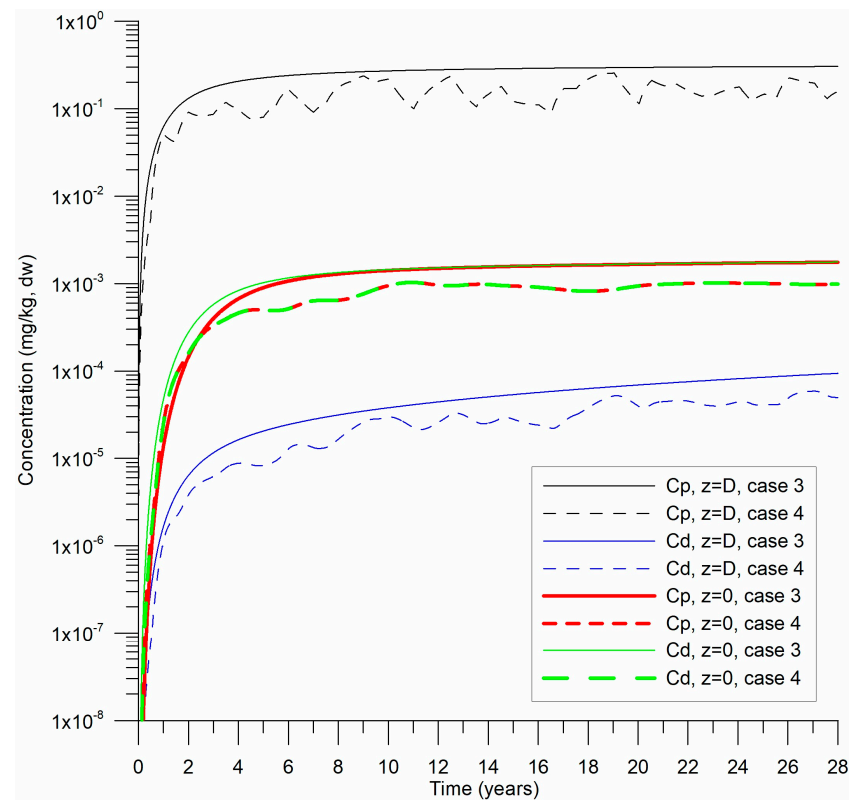


Figure 6. Temporal evolution of particulate (C_p) and dissolved (C_d) HHM concentrations at the variable bed level $D(t)$ and at the basal level ($z = 0$) of the bottom substrate for Cases 3 and 4.

4.2. Dimensionless Analysis and HHM Dynamics

To perform an analysis of the systems in Equations (1) and (6)–(9), dimensionless variables were introduced as follows:

$$\begin{aligned}\tilde{C}_d &= \frac{C_d}{C_{bg}}; \tilde{C}_p = \frac{C_p}{C_{bg}}; \tilde{t}_1 = \frac{t}{T_1}; \tilde{t}_2 = \frac{t}{T_2}; \tilde{t}_3 = \frac{t}{T_3}; \tilde{z} = \frac{z}{D}; \frac{\tilde{t}_2}{\tilde{t}_1} = \frac{2\gamma D^2}{\alpha_S \nu} = a; \\ \tilde{C}_{p0} &= \frac{C_{p0}}{C_{bg}}; \frac{\tilde{t}_1}{\tilde{t}_3} = \frac{w_g D}{\alpha_S \nu} = \beta; \tilde{D} = \frac{D}{D_0}; \zeta = \frac{\alpha_S \nu}{u_* D}; \tilde{C}_{p0} = \frac{C_{p0}}{C_{bg}}.\end{aligned}$$

The “~” symbol implies a dimensionless variable.

The systems originally presented in Equations (6) and (7), along with their respective conditions (8) and (9), are reformulated in dimensionless form and have been renumbered consecutively as Equations (12)–(15), as follows:

$$\frac{\partial \tilde{C}_p}{\partial \tilde{t}_1} = -a(\tilde{C}_p - \tilde{C}_d) - \beta \tilde{C}_{p0} \delta(\tilde{z} - \tilde{D}), \quad (12)$$

$$\frac{\partial \tilde{C}_d}{\partial \tilde{t}_1} = a(\tilde{C}_p - \tilde{C}_d) + \frac{\partial}{\partial \tilde{z}} \left(\tilde{\alpha}_S \frac{\partial \tilde{C}_d}{\partial \tilde{z}} \right), \quad (13)$$

$$C_D^{\frac{1}{2}} \tilde{C}_d + \zeta \frac{\partial \tilde{C}_d}{\partial \tilde{z}} = 0, \text{ at } \tilde{z} = \tilde{D} \quad (14)$$

$$\frac{\partial \tilde{C}_d}{\partial \tilde{z}} = 0, \text{ at } \tilde{z} = 0. \quad (15)$$

Adding Systems (12) and (13) and using conditions (14) and (15), the results are as follows:

$$\int_0^{\tilde{D}} \frac{\partial(\tilde{C}_p + \tilde{C}_d)}{\partial \tilde{t}_1} d\tilde{z} = |\beta| \tilde{C}_{p0} - \frac{1}{\zeta} \tilde{C}_D^2 \tilde{C}_d \left(\tilde{z} = \tilde{D} \right). \quad (16)$$

Applying Leibniz's rule and reformulating Equation (1) in terms of "fast" time \tilde{t}_1 , we obtain the following:

$$\frac{\partial \tilde{D}}{\partial \tilde{t}_1} = \frac{C_v}{\{|\beta|(1-n)\}} \quad (17)$$

The temporal variation in the total HHM concentration of sediments over the entire extent of its layers can be defined by the following equation:

$$\frac{\partial}{\partial \tilde{t}_1} \int_0^{\tilde{D}} (\tilde{C}_p + \tilde{C}_d) d\tilde{z} = |\beta| \tilde{C}_{p0} - \frac{1}{\zeta} \tilde{C}_D^2 \tilde{C}_d \left(\tilde{z} = \tilde{D} \right) + \frac{C_v}{\{|\beta|(1-n)\} (\tilde{C}_p + \tilde{C}_d)} \Big|_{\tilde{D}}. \quad (18)$$

The first term on the right-hand side of Equation (18) represents the input of HHMs in C_p into the sediment column, while the second term accounts for their loss through exchange with the overlying water in the C_d . The final term corresponds to the increase in the total HHM concentration due to changes in substrate thickness and its redistribution in the column. This term was considered less relevant when the T_3 scale represented a slow time relative to T_1 and T_2 . Within the same body of water, as exemplified by CB, the T_3 scale is spatially variable.

If $\frac{\partial \tilde{D}}{\partial \tilde{t}_1} \approx 0$ for the "fast" time in System (17), then systems (12)–(15) are represented as parabolic equations whose asymptotes in time are $\tilde{C}_p = \tilde{C}_d$. Steady-state conditions are possible only if the particle sedimentation process stops.

For $\rightarrow \infty$, $\frac{\partial}{\partial \tilde{z}} \left(\tilde{\alpha}_S \frac{\partial \tilde{C}_d}{\partial \tilde{z}} \right) = 0$, considering condition (15) at a given level, the molecular flow is equal to zero throughout the substrate.

In this case, $\tilde{C}_p = \tilde{C}_d = 1 \forall t$ (background concentration). The only reason this did not occur throughout the entire sediment column is the permanent entry of HHMs, owing to their precipitation on particles at the bottom and the exchange of the diluted phase with the water column at the same vertical level.

The simulated sedimentation rates ranged from 0.5 m per 25 years (low deposition) to 10 m per 25 years (at the river mouth). Figure 1 presents the variability in sedimentation across CB, highlighting three depositional zones: Dique Channel mouth: 10 m/25 y; the central bay: 1 m/25 y; and the northern sector: 0.5 m/25 y. Therefore, the 1D model should be applied at each calculation node of a 3D hydrodynamic mesh, with local scales adjusted accordingly.

The universality of the proposed model lies in its formulation using dimensionless variables and scale parameters. The analysis of dimensionless equations (Equations (12)–(15)) allows for a broad spectrum of environmental conditions. These ranges reflect both the intra-basin variability within CB, such as differences between river mouth and inner-bay sedimentation rates, and potential conditions in other estuarine systems. This dimensional analysis enables the model to be applied across geographically distinct water bodies, provided that the local sedimentation dynamics and hydro-sedimentary conditions are within comparable parameter bounds.

Considering the timescale variation in the main processes, the desorption rate, the average speed of sediment settling by gravity, and the molecular viscosity of water were fixed. The thickness of the sediment layer and its porosity (through the Schmidt number) varied within reasonable limits, characterizing CB as an example of an estuary. The resulting values of the dimensionless parameters for systems (12)–(15) were $a = 10^{-3}$ to 10^3 ; $\beta = 10^2$ to 10^4 ; $\zeta/C_D^{\frac{1}{2}} = 0.25$ (10^{-1} – 10^{-5}); and $\tilde{\alpha}_S = 10^{-2}$ to 10^2 .

Under these conditions, Equations (12) and (13) can present multiple scenarios of HHM dynamics because the ratios of scale $\frac{\tilde{t}_2}{\tilde{t}_1}$ and $\frac{\tilde{t}_1}{\tilde{t}_3}$ change four to six orders of magnitude.

In the case where the parameter $a = \frac{\tilde{t}_2}{\tilde{t}_1}$, the scales become inverted. Regarding condition

(14), the relationship $\zeta/C_D^{\frac{1}{2}} \ll 1$ implied an abrupt gradient $\frac{\partial \tilde{C}_d}{\partial \tilde{z}}$, which was observed in Figure 4 at the interface between sediments and water. This detail was not observed in the measurements of HHMs in sediments because the laboratories analyze the total concentrations, where $C_d/K_d + C_p$, and the C_p concentration predominates in the samples.

4.3. Model Assumptions, Limitations, and Ecological Implications

While CB served as a reference system to contextualize parameter ranges and model outputs, this study was not designed for site-specific application or empirical calibration. Rather, the model was developed to explore general physical processes governing HHM desorption and accumulation in estuarine sediments. Field data from CB, including reported sedimentation rates and Hg concentrations, were used qualitatively to guide parameter selection and verify that simulated C_{bg} remained within empirically observed values, supporting the model's realism under estuarine conditions.

The proposed 1D model was developed under the assumptions of continuous sedimentation without bottom erosion events. Technically, erosion could be easily included in the model; however, it may be difficult to control over extended periods of sediment dynamics. Changes in the porosity and tortuosity were also considered, which influence HHM transport and accumulation. These mechanisms may require a rheological model. Since the model operated under the assumption that the muddy substrate was not in motion, no assumption of the fluid type or the Newtonian fluid approximation is required.

A notable limitation of the current model is the assumption of a constant sedimentation velocity (w_g), whereas sedimentation processes in estuarine environments typically exhibit considerable spatial complexity. For instance, Figure 1 highlights sedimentation rates in CB varying by an order of magnitude between the Dique Channel mouth (10 m/25 y) and the northern bay sector (0.5 m/25 y). Such variations result from a combination of (a) bed load transport, (b) the precipitation of suspended particles, and (c) the flocculation of fine particles induced by brackish water salinity gradients. Determining the dominant mechanism among these and assessing the impact of wash load transport on sediment distribution throughout the bay remain challenging. Detailed geographic-specific analysis and further refinement of sedimentation mechanisms given in Equation (1) would thus enhance the model accuracy and applicability.

This modeling approach addresses a critical gap in the representation of sediment processes, particularly the understanding of C_{bg} of HHMs in estuarine sediments, by integrating transport and reaction processes with site-specific hydro-sedimentary influences, often simplified in traditional frameworks. The relevance of C_{bg} lies in its strong association with toxicological thresholds, bioavailability, and long-term ecological risks related to HHM pollution. Although a 1D framework offers notable advantages in computational efficiency, it limits horizontal transport and spatial interactions across estuarine gradients.

Future initiatives could benefit from integrating diagenetic and hydrodynamic models to support evidence-based environmental management for preserving estuarine ecosystems.

5. Conclusions

Under physically valid assumptions, a novel 1D mathematical model was developed to simulate HHM dynamics in estuarine sediments, with broad applicability to water bodies influenced by HHM contamination. This numerical framework advances prior approaches by integrating coupled transport-reaction processes while dynamically accounting for porosity and tortuosity. Unlike conventional models, this approach includes molecular diffusion (T_1), desorption (T_2), sedimentation (T_3), and water-turbulence exchange (T_4) as a distinct method to estimate HHM C_{bg} . A notable innovation is the separation of C_d and C_p , reaching an asymptotic equilibrium ($C_d = C_p = C_{bg}$) at the sediment base ($z = 0$). This mathematical formulation has not been previously reported in existing sediment models.

The C_{bg} for Hg in CB ranged from 1.0 to 2.4 mg kg⁻¹ dw, providing a valuable reference for future ecological risk assessments, pollution indexing, and numerical model calibration in estuarine sediments. C_{bg} of Hg were characterized by very slow desorption. Particularly, C_{bg} values did not remain constant but exhibited a drift, influenced by limited exchange with upper layers and overlying water. These findings may improve ecological risk assessment, environmental monitoring, and policy formulation to mitigate HHM impacts in CB and similar contaminated ecosystems.

Spatial and temporal variability in C_{bg} arises from local sediment dynamics, precisely variations in precipitation rates, highlighting the need for zone-specific assessments within the same water body. Consequently, the 1D model can be applied to each node of the general hydrodynamic model of the basin.

The observed drift in C_{bg} values demonstrates that profiling sediment layers dated with ¹⁴C does not necessarily reflect historical in situ concentrations, as reported by Fukue et al. [44]. This issue draws attention and stimulates future research using inverse models to restore HHM ancient profiles from in situ measurements.

The 1D model would be implemented as an interface between the water column and the consolidated substrate. This intermediate layer would capture processes at the sediment–water interface, transitioning from Newtonian fluid properties in the water–sediment upper layer of the bottom to solid substrate characteristics. The model acts as a universal boundary condition applicable across diverse aquatic systems receiving HHM contamination. However, site-specific calibration may be necessary due to local sedimentological and hydrodynamic conditions.

Future works will focus on integrating the 1D model into a 3D hydrodynamic framework to continuously simulate the long-term fate of sediments and HHMs to compare the model's stratification predictions to in situ measurements of the vertical substrate. Such advancements could significantly aid in developing more effective management strategies to mitigate HHM pollution in coastal marine environments.

Author Contributions: Conceptualization, W.T.G.C., S.L. and K.K.; methodology, W.T.G.C., S.L. and K.K.; software, S.L.; validation, S.L. and K.K.; formal analysis, W.T.G.C.; investigation, W.T.G.C., S.L. and K.K.; resources, W.T.G.C., S.L. and K.K.; data curation, W.T.G.C.; writing—original draft preparation, W.T.G.C. and S.L.; writing—review and editing, S.L. and K.K.; visualization, W.T.G.C. and S.L.; supervision, K.K.; project administration, K.K.; funding acquisition, K.K. All authors have read and agreed to the published version of the manuscript.

Funding: This research was funded by the Korea Institute of Ocean Science and Technology, Republic of Korea, grant number PEA0301, and by the Ministry of Oceans and Fisheries, Republic of Korea, grant number KIMST-20220027. The authors gratefully acknowledge this support.

Institutional Review Board Statement: Not applicable.

Informed Consent Statement: Not applicable.

Data Availability Statement: Data available on request from the authors.

Acknowledgments: We thank everyone who was related to this research and the anonymous reviewers, whose valuable comments led to the enhancement of the final version of this manuscript. We would like to express our special gratitude to the Korea Institute of Ocean Science and Technology (KIOST), Republic of Korea, and the Colombian Navy for their support. Graphical abstract created in <https://BioRender.com>.

Conflicts of Interest: The authors declare no conflicts of interest.

Appendix A

Without the source term and molecular diffusion in a closed system, Equations (6) and (7) can be expressed as follows:

$$\frac{\partial C_p}{\partial t} = -\gamma(C_p - C_d) \quad (\text{A1})$$

$$\frac{\partial C_d}{\partial t} = \gamma(C_p - C_d), \quad (\text{A2})$$

This represents the desorption from the particulate to the dissolved form of the HHMs, with

$$\frac{\partial(C_p + C_d)}{\partial t} = 0$$

Assuming the initial conditions $C_p(t=0) = C_0$ and $C_d(t=0) = 0$, the respective analytical solution of the system (Equations (A1) and (A2)) becomes the following:

$$C_p(t) = \frac{C_0(1 + e^{-2\gamma t})}{2}; C_d(t) = \frac{C_0(1 - e^{-2\gamma t})}{2}, \quad (\text{A3})$$

until it reaches an equilibrium, where $C_p = C_d = \frac{C_0}{2}$ for $t \rightarrow \infty$. The characteristic scale of this process, given in Equation (4), according to Equation (A3) is $T_2 = \frac{1}{2\gamma}$.

Appendix B

To specify the boundary conditions for Equation (7) at the bottom surface, a flux equilibrium was established for the dissolved components of the HHMs:

$$-\overline{w'C'} + \nu \frac{\partial \overline{C}}{\partial z} = \alpha_S \nu \frac{\partial \overline{C}_d}{\partial z} \quad (\text{A4})$$

Here, the first and second terms on the left-hand side represent the turbulent and molecular fluxes of the HHMs with concentrations \overline{C} in the water, respectively. The term on the right-hand side is the molecular diffusion flux of the substance in the sediments.

The sum of the turbulent and molecular fluxes was constant in a relatively thick layer, known as the near-surface bulk layer or “layer of constant fluxes”. This could be parameterized based on the K-theory of turbulence by defining the flux q within the logarithmic profile of the substance:

$$q = \frac{(\overline{C} - C_d) \kappa u_*}{\ln\left(\frac{z}{z_0}\right)}, \quad (\text{A5})$$

where κ = Karman constant ($\kappa = 0.41$); u_* is the friction (dynamic) velocity in the near-surface layer; z_0 is the roughness parameter. In this case, z extends from the bottom surface z_0 upwards and is fixed with a reference value \bar{C} of concentrations.

Introducing the drag coefficient C_D and assuming that the concentration in water is $\bar{C} = 0$ in Equation (A5), and based $\bar{C} \ll C_d$, Equation (A4) gives the following:

$$-C_d C_D^{\frac{1}{2}} u_* = \alpha_S \nu \frac{\partial \bar{C}_d}{\partial z}, \quad (\text{A6})$$

which is Equation (8) when $A = C_D^{1/2} u_*$.

The fact that $\bar{C} \ll C_d$ in the water column was justified under the assumption that the volumetric sediment concentrations in the water were less than 10^{-4} . In an extreme hypothetical scenario, where equilibrium is reached between the HHMs in the water column, encompassing both C_p and C_d , the concentration \bar{C} represents no more than 0.01% of the C_p .

Appendix C

Generally, the molecular Schmidt number, Sc , characterizes the relationship between the molecular viscosity of water and the molecular diffusion of substances; it measures how fast the “diffusion of momentum” occurs relative to other fluid properties. Substances with a water temperature of approximately $Sc = 10$ can increase by one or two orders of magnitude [36].

The Schmidt number is associated with the porosity and tortuosity of a fluid composed of liquid and bottom sediments. Porosity and tortuosity are considered to play major roles in the increase of this number. In the proposed study by Maerki et al. [45], the molecular flow (2) was identified as follows:

$$Q = n \chi_S \frac{\partial C_d}{\partial z} = n \chi_0 \theta^{-2} \frac{\partial C_d}{\partial z} = F^{-1} \chi_0 \frac{\partial C_d}{\partial z}, \quad (\text{A7})$$

where n represents porosity, θ characterizes tortuosity, and F combines the effect of both; χ_S and χ_0 are the molecular diffusion coefficients with and without sediment particles, respectively.

If $\chi_0 = \nu$ and all diffusion effects (substance, porosity, and tortuosity) are assigned to the Sc number, then $Sc = F$. Based on Maerki et al. [45], we conclude the following:

$$Sc = 1.02n^{-m} \quad (\text{A8})$$

where $m > 1$ ($m = 1.81$ in the cited work).

Consequently, the Sc value depends on the substrate level, residence time, and compaction of the sediment, among other factors. Shen and Chen [46] provided further details on the parameterizations of these effects in sediments.

References

1. Abdelmonem, B.H.; Kamal, L.T.; Elbaz, R.M.; Khalifa, M.R.; Abdelnaser, A. From Contamination to Detection: The Growing Threat of Heavy Metals. *Heliyon* **2025**, *11*, e41713. [[CrossRef](#)] [[PubMed](#)]
2. Proshad, R.; Asha, S.M.A.A.; Tan, R.; Lu, Y.; Abedin, M.A.; Ding, Z.; Zhang, S.; Li, Z.; Chen, G.; Zhao, Z. Machine Learning Models with Innovative Outlier Detection Techniques for Predicting Heavy Metal Contamination in Soils. *J. Hazard. Mater.* **2025**, *481*, 136536. [[CrossRef](#)] [[PubMed](#)]
3. Liu, H.; Ding, C.; Zhang, G.; Guo, Y.; Song, Y.; Thangaraj, S.; Zhang, X.; Sun, J. Dissolved and Particulate Heavy Metal Pollution Status in Seawater and Sedimentary Heavy Metals of the Bohai Bay. *Mar. Environ. Res.* **2023**, *191*, 106158. [[CrossRef](#)] [[PubMed](#)]
4. Liu, Q.; Yang, P.; Hu, Z.; Shu, Q.; Chen, Y. Identification of the Sources and Influencing Factors of the Spatial Variation of Heavy Metals in Surface Sediments along the Northern Jiangsu Coast. *Ecol. Indic.* **2022**, *137*, 108716. [[CrossRef](#)]

5. Zhou, L.; Wu, F.; Meng, Y.; Byrne, P.; Ghomshei, M.; Abbaspour, K.C. Modeling Transport and Fate of Heavy Metals at the Watershed Scale: State-of-the-Art and Future Directions. *Sci. Total Environ.* **2023**, *878*, 163087. [\[CrossRef\]](#)
6. Schnoor, J.; Sato, C.; McKechnie, D.; Sahoo, D. *Processes, Coefficients, and Models for Simulating Toxic Organics and Heavy Metals in Surface Waters*; EPA/600/3-87/015; Department of Civil and Environmental Engineering, University of Iowa: Iowa City, IA, USA, 1987.
7. Sun, Y.; Zhao, Y.; Hao, L.; Zhao, X.; Lu, J.; Shi, Y.; Ma, C.; Li, Q. Application of the Partial Least Square Regression Method in Determining the Natural Background of Soil Heavy Metals: A Case Study in the Songhua River Basin, China. *Sci. Total Environ.* **2024**, *918*, 170695. [\[CrossRef\]](#)
8. Luo, M.; Kang, X.; Liu, Q.; Yu, H.; Tao, Y.; Wang, H.; Niu, Y.; Niu, Y. Research on the Geochemical Background Values and Evolution Rules of Lake Sediments for Heavy Metals and Nutrients in the Eastern China Plain from 1937 to 2017. *J. Hazard. Mater.* **2022**, *436*, 129136. [\[CrossRef\]](#)
9. Kuang, Z.; Shi, Z.; Wang, H.; Du, S.; Gong, H.; Liu, Q.; Gu, Y.; Fan, Z.; Huang, H.; Wang, S. Bioavailability of Trace Metals in Sediments from Daya Bay Nature Reserve: Spatial Variation, Controlling Factors and the Exposure Risk Assessment for Aquatic Biota. *Ecol. Indic.* **2024**, *169*, 112789. [\[CrossRef\]](#)
10. Wu, Y.; Falconer, R.; Lin, B. Modelling Trace Metal Concentration Distributions in Estuarine Waters. *Estuar. Coast. Shelf Sci.* **2005**, *64*, 699–709. [\[CrossRef\]](#)
11. Chang, S.; Han, L.; Chen, R.; Liu, Z.; Fan, Y.; An, X.; Zhai, Y.; Wu, P.; Wang, T. Vulnerability Assessment of Soil Cadmium with Adsorption–Desorption Coupling Model. *Ecol. Indic.* **2023**, *146*, 109904. [\[CrossRef\]](#)
12. Ristea, E.; Pârvolescu, O.C.; Lavric, V.; Oros, A. Assessment of Heavy Metal Contamination of Seawater and Sediments Along the Romanian Black Sea Coast: Spatial Distribution and Environmental Implications. *Sustainability* **2025**, *17*, 2586. [\[CrossRef\]](#)
13. Yao, J.; Liu, W.; Chen, Z. Numerical Solution of a Moving Boundary Problem of One-Dimensional Flow in Semi-Infinite Long Porous Media with Threshold Pressure Gradient. *Math. Probl. Eng.* **2013**, *2013*, 384246. [\[CrossRef\]](#)
14. Bhandari, A.; Surampalli, R.Y.; Champagne, P.; Ong, S.K.; Tyagi, R.D.; Lo, I.M.C. *Remediation Technologies for Soils and Groundwater*; American Society of Civil Engineers (ASCE): Reston, VA, USA, 2007; Volume 60, pp. 1–449. [\[CrossRef\]](#)
15. Liang, H.Y.; Zhang, Y.H.; Du, S.L.; Cao, J.L.; Liu, Y.F.; Zhao, H.; Ding, T.T. Heavy Metals in Sediments of the River-Lake System in the Dianchi Basin, China: Their Pollution, Sources, and Risks. *Sci. Total Environ.* **2024**, *957*, 177652. [\[CrossRef\]](#)
16. Lonin, S.; Andrade, C.A.; Monroy, J. Wave Climate and the Effect of Induced Currents over the Barrier Reef of the Cays of Albuquerque Island, Colombia. *Sustainability* **2022**, *14*, 6069. [\[CrossRef\]](#)
17. Boudreau, B.P. *Diagenetic Models and Their Implementation*; Springer: Berlin/Heidelberg, Germany, 1998; Volume 15, ISBN 978-3-642-64399-6.
18. Lynch, D.R.; Officer, C.B. Nonlinear Parameter Estimation for Sediment Cores. *Chem. Geol.* **1984**, *44*, 203–225. [\[CrossRef\]](#)
19. Nicolis, C. Tracer Dynamics in Ocean Sediments and the Deciphering of Past Climates. *Math. Comput. Model.* **1995**, *21*, 27–38. [\[CrossRef\]](#)
20. Sun, Y.; Yang, J.; Li, K.; Gong, J.; Gao, J.; Wang, Z.; Cai, Y.; Zhao, K.; Hu, S.; Fu, Y.; et al. Differentiating Environmental Scenarios to Establish Geochemical Baseline Values for Heavy Metals in Soil: A Case Study of Hainan Island, China. *Sci. Total Environ.* **2023**, *898*, 165634. [\[CrossRef\]](#)
21. Jung, J.M.; Kim, C.J.; Chung, C.S.; Kim, T.; Gu, H.S.; Kim, H.E.; Choi, K.Y. Applying New Regional Background Concentration Criteria to Assess Heavy Metal Contamination in Deep-Sea Sediments at an Ocean Dumping Site, Republic of Korea. *Mar. Pollut. Bull.* **2024**, *200*, 116065. [\[CrossRef\]](#)
22. Olivero-Verbel, R.; Eljarrat, E.; Johnson-Restrepo, B. Organophosphate Ester Flame Retardants in Sediments and Marine Fish Species in Colombia: Occurrence, Distribution, and Implications for Human Risk Assessment. *Mar. Pollut. Bull.* **2025**, *213*, 117654. [\[CrossRef\]](#)
23. Caballero-Gallardo, K.; Alcala-Orozco, M.; Barraza-Quiroz, D.; De la Rosa, J.; Olivero-Verbel, J. Environmental Risks Associated with Trace Elements in Sediments from Cartagena Bay, an Industrialized Site at the Caribbean. *Chemosphere* **2020**, *242*, 125173. [\[CrossRef\]](#)
24. Tosić, M.; Restrepo, J.D.; Lonin, S.; Izquierdo, A.; Martins, F. Water and Sediment Quality in Cartagena Bay, Colombia: Seasonal Variability and Potential Impacts of Pollution. *Estuar. Coast. Shelf Sci.* **2019**, *216*, 187–203. [\[CrossRef\]](#)
25. Romero-Murillo, P.; Gallego, J.L.; Leignel, V. Marine Pollution and Advances in Biomonitoring in Cartagena Bay in the Colombian Caribbean. *Toxics* **2023**, *11*, 631. [\[CrossRef\]](#) [\[PubMed\]](#)
26. Tosić, M.; Ángel, J.D.R. Sustainability Impacts of Sediments on the Estuary, Ports, and Fishing Communities of Cartagena Bay, Colombian Caribbean. *Wiley Interdiscip. Rev. Water* **2023**, *11*, e1709. [\[CrossRef\]](#)
27. Cano, W.T.G.; Kim, K. How to Achieve Sustainably Beneficial Uses of Marine Sediments in Colombia? *Sustainability* **2022**, *14*, 14821. [\[CrossRef\]](#)
28. Tosić, M.; Martins, F.; Lonin, S.; Izquierdo, A.; Restrepo, J.D. Hydrodynamic Modelling of a Polluted Tropical Bay: Assessment of Anthropogenic Impacts on Freshwater Runoff and Estuarine Water Renewal. *J. Environ. Manag.* **2019**, *236*, 695–714. [\[CrossRef\]](#)

29. Andrade, C.; Thomas, Y.F.; Lonin, S.; Parra, C.; Kunesch, S.; Menanteau, L.; Andriau, A.; Piñeres, C.; Velasco, S. Aspectos morfodinámicos de la bahía de Cartagena de Indias. *Bol. Cient. CIOH* **2004**, *22*, 90–104. [[CrossRef](#)]
30. Thomas, Y.F.; Cesaraccio, M.; Kunesch, S.; Andrieu, A.; Ménanteau, L.; Andrade, C.; Lonin, S.; Parra, C.; Pineres, C.; Velasco, S.P. Étude Morphodynamique de La Baie de Carthagène Des Indes, Colombie. In *Milieux Littoraux, Nouvelles Perspectives D' Études*; L'Harmattan: Paris, France, 2005; pp. 171–191.
31. Thomas, Y.F.; Ménanteau, L.; Kunesch, S.; Cesaraccio, M.; Andrade, C.; Lonin, S.; Parra, C. Le delta du canal du Dique (baie de Carthagène des Indes, Colombie). Modélisation géomorphologique et sédimentologique. In Proceedings of the Colloque International Interactions-Nature-Sociétés, Analyses et Modèles, La Baule-Escoublac, France, 3–6 May 2006; pp. 1–7.
32. Van Rijn, L.C. *Principles of Sediment Transport in Rivers, Estuaries and Coastal Seas*; Aqua Publications: Amsterdam, The Netherlands, 1993.
33. Bartlett, P.; Craig, P. Total Mercury and Methyl Mercury Levels in British Estuarine Sediments—II. *Water Res.* **1981**, *15*, 37–47. [[CrossRef](#)]
34. Boudreau, B.P. The Diffusive Tortuosity of Fine-Grained Unlithified Sediments. *Geochim. Cosmochim. Acta* **1996**, *60*, 3139–3142. [[CrossRef](#)]
35. Ghanbarian, B.; Hunt, A.G.; Ewing, R.P.; Sahimi, M. Tortuosity in Porous Media: A Critical Review. *Soil Sci. Soc. Am. J.* **2013**, *77*, 1461–1477. [[CrossRef](#)]
36. Monin, A.S.; Yaglom, A.M. *Statistical Fluid Mechanics: The Mechanics of Turbulence, Volume 1*; MIT Press: Cambridge, MA, USA, 1973; Volume 60.
37. Orani, A.M.; Vassileva, E.; Azemard, S.; Alonso-Hernandez, C. Trace Elements Contamination Assessment in Marine Sediments from Different Regions of the Caribbean Sea. *J. Hazard. Mater.* **2020**, *399*, 122934. [[CrossRef](#)] [[PubMed](#)]
38. Olivero-Verbel, J.; Caballero-Gallardo, K.; Torres-Fuentes, N. Assessment of Mercury in Muscle of Fish from Cartagena Bay, a Tropical Estuary at the North of Colombia. *Int. J. Environ. Health Res.* **2009**, *19*, 343–355. [[CrossRef](#)] [[PubMed](#)]
39. Marchuk, G.I.; Kagan, B.A. *Ocean Tides: Mathematical Models and Numerical Experiments*; Pergamon Press: Oxford, UK, 1984.
40. Pintilie, S.; Brânză, L.; Bețianu, C.; Pavel, L.V.; Ungureanu, F.; Gavrilescu, M. Modelling and Simulation of Heavy Metals Transport in Water and Sediments. *Environ. Eng. Manag. J.* **2007**, *6*, 153–161. [[CrossRef](#)]
41. Luo, P.; Luo, M.; Li, F.; Qi, X.; Huo, A.; Wang, Z.; He, B.; Takara, K.; Nover, D.; Wang, Y. Urban Flood Numerical Simulation: Research, Methods and Future Perspectives. *Environ. Model. Softw.* **2022**, *156*, 105478. [[CrossRef](#)]
42. Liu, Q.; Jia, Z.; Liu, G.; Li, S.; Hu, J. Assessment of Heavy Metals Remobilization and Release Risks at the Sediment-Water Interface in Estuarine Environment. *Mar. Pollut. Bull.* **2023**, *187*, 114517. [[CrossRef](#)]
43. He, L.; Chen, G.; Wang, X.; Shen, J.; Zhang, H.; Lin, Y.; Shen, Y.; Lang, F.; Gong, C. Pollution Characteristics and Risk Assessment of Heavy Metals in the Sediments of the Inflow Rivers of Dianchi Lake, China. *Toxics* **2024**, *12*, 322. [[CrossRef](#)]
44. Fukue, M.; Yanai, M.; Sato, Y.; Fujikawa, T.; Furukawa, Y.; Tani, S. Background Values for Evaluation of Heavy Metal Contamination in Sediments. *J. Hazard. Mater.* **2006**, *136*, 111–119. [[CrossRef](#)]
45. Maerki, M.; Wehrli, B.; Dinkel, C.; Müller, B. The Influence of Tortuosity on Molecular Diffusion in Freshwater Sediments of High Porosity. *Geochim. Cosmochim. Acta* **2004**, *68*, 1519–1528. [[CrossRef](#)]
46. Shen, L.; Chen, Z. Critical Review of the Impact of Tortuosity on Diffusion. *Chem. Eng. Sci.* **2007**, *62*, 3748–3755. [[CrossRef](#)]

Disclaimer/Publisher's Note: The statements, opinions and data contained in all publications are solely those of the individual author(s) and contributor(s) and not of MDPI and/or the editor(s). MDPI and/or the editor(s) disclaim responsibility for any injury to people or property resulting from any ideas, methods, instructions or products referred to in the content.